Bull. Mater. Sci., Vol. 40, No. 7, December 2017, pp. 1309–1318
https://doi.org/10.1007/s12034-017-1493-y

© Indian Academy of Sciences

Synthesis, characterization and catalytic application of Ni catalysts supported on alumina–zirconia mixed oxides

J ÁNGEL-SOTO[1,*], M MARTÍNEZ-ROSALES[2], P ÁNGEL-SOTO[3] and A ZAMORATEGUI-MOLINA[4]

[1]Department of Chemical Engineering, University of Guanajuato, Noria Alta S/N, 36050 Guanajuato, Mexico
[2]Department of Chemistry, University of Guanajuato, Noria Alta S/N, 36050 Guanajuato, Mexico
[3]Department of Industrial Engineering, Technological Institute of Leon, Industrial Julian de Obregon, 37290 León, Mexico
[4]Department of Civil Engineering, University of Guanajuato, Avenida Juárez No. 77, Zona Centro, 36000 Guanajuato, Mexico
*Author for correspondence (jasoto@ugto.mx)

MS received 31 October 2016; accepted 20 March 2017; published online 11 November 2017

Abstract. Alumina and alumina–zirconia mixed oxides were compared as supports to prepare nickel catalysts. The oxides were prepared by the sol–gel method using aluminum tri-sec-butoxide and zirconium (IV) propoxide as precursors, and its physicochemical properties were determined by BET, TGA, DTA, XRD, SEM and TEM. The catalysts of nickel were obtained by the impregnation of the supports with nickel nitrate (10 wt%) and were heat-treated at 700°C. The specific area of the supports and catalysts decreased with the increase in the zirconia content in agreement with the crystalline phase formed. TEM micrographs of nickel catalysts revealed particles in the size range of 10–30 nm. The Ni/Al_2O_3–ZrO_2 catalysts were tested in the steam reforming reaction of ethanol (SRE) at 500°C, and the obtained results suggest that the differences in catalytic activities depended on the content of ZrO_2. The selectivity towards H_2 was ∼56% for the named catalyst Ni–Al–0.25Zr.

Keywords. Alumina; alumina–zirconia mixed oxides; sol–gel method; nickel catalysts; steam reforming.

1. Introduction

The catalysts γ-Al_2O_3 is widely used because it can provide high surface area for many applications [1,2]. One of the most important factors in γ-Al_2O_3 utilization is a controlled pore-size distribution and its thermal stability [3].

Zirconia is a essential material with growing application in heterogeneous catalysis, both as an active material or as a support. It is also a relevant material in adsorption [4]. Fine particles of zirconia show a better wear resistance and lower resistance to diffusion, while nanocrystalline zirconia has a high adsorptive capacity, which is favourable for catalysis and adsorption applications, respectively [5].

The oxide of zirconium is characterized by high chemical resistance and is stable over a wide temperature range. Furthermore, it possesses both acidic and basic centres. Therefore, it can act as a basic or an acid catalyst, and hence, additional attempts are made to improve the properties of zirconia and alumina supports forming mixed oxides of Al–Zr [6]. The alumina mixed oxides present higher catalytic behaviour than the pure ZrO_2 or Al_2O_3, because they present more thermal stability, medium acidity and moderate surface area [7–9].

Several methods are used to synthesize the catalyst supports, such as coprecipitation, plasma, homogeneous precipitation and sol–gel methods, which are all reported in the literature. In this regard, the sol–gel method can control the pore size, surface area and high purity materials better than other preparation methods, such as the coprecipitation method.

In recent years, the Ni-based catalysts on alumina–zirconia have attracted much interest owing to the fact that nickel has a low cost and can break C–C bonds in reforming reactions of hydrocarbons [10–12]. In this type of reaction, the catalysts based on noble metals such as Pd, Rh, Pt, etc. are less sensitive to coke formation, compared to nickel-based catalysts. However, the catalysts have the disadvantage of high cost and limited availability, which is important in the development of active and stable nickel catalysts to different research groups [13–15].

The aim of the present work is to prepare and characterize Ni catalysts supported over Al_2O_3–ZrO_2 mixed oxides, also to study the effect of zirconia content in the obtained catalysts, performing reactions with them in the steam reforming case at 500°C. In this study, the alumina–zirconia supports were synthesized by the sol–gel method using three different molar ratio samples of Al_2O_3/ZrO_2.

2. Methods and procedures

2.1 *Synthesis of Al_2O_3–ZrO_2 mixed oxides and Ni-based catalyst*

The Al_2O_3–ZrO_2 mixed oxides synthesized by the sol–gel method used the following procedure with a molar ratio of 80/30/0.3/1 (alcohol/water/acid/alkoxide). Appropriate quantities of aluminum tri-sec-butoxide (97%, Aldrich) and anhydrous ethanol (94.2%, J T Baker) were mixed in a reactor vessel with continuous stirring for 20 min under an inert atmosphere of nitrogen. In another vessel-reactor, zirconium (IV) propoxide (70 wt%, Aldrich) and the appropriate amount of ethanol were mixed under an inert atmosphere of nitrogen, stirred briskly for 20 min. Then, both solutions were blended by stirring the mixture vigorously for 2 h at room temperature until a clear solution was obtained. To this solution, an aqueous solution of HNO_3 (65%, J T Baker) was added dropwise at room temperature. The gel formed was aged for 24 h at room temperature. The starting heat treatment step is to dry the powder up to 120°C for 1 h at a heating rate of 1°C min^{-1} starting at room temperature. The resulting powder was finally heat-treated up to 700°C for 2 h at a heating rate of 0.5°C min^{-1}. Three samples of Al_2O_3–ZrO_2 mixed oxides were prepared with different molar ratios of Al_2O_3/ZrO_2, $X = 0.25{:}1$, 1:1, 1:0.25, which are further denoted as 0.25Al–Zr, Al–Zr and Al–0.25Zr. Al_2O_3 support was obtained using the procedure described above.

The supported nickel catalysts were prepared by impregnating the Al_2O_3–ZrO_2 and Al_2O_3 support with an aqueous solution of $Ni(NO_3)_2 \cdot 6H_2O$ (J T Baker) using a nickel load of 10 wt% for all the samples. The fresh catalysts were dried at room temperature for 24 h and were then calcined using the same temperature ramp which is utilized previously for the supports. The catalysts are denoted as Ni–0.25Al–Zr, Ni–Al–Zr, Ni–Al–0.25Zr and Ni–Al_2O_3.

2.2 *Characterization of supports and catalysts*

Textural characterization of the supports and catalysts samples were made by N_2 adsorption–desorption using a Micromeritics ASAP 2010 instrument. The pore-size distributions were determined by the Barret–Joyner–Hallenda (BJH) method, applied to the desorption branch-profile of the nitrogen isotherm. The crystal structure of the different supports and catalysts was determined by an Inel EQUINOX 3000D diffractometer using monochromatic CuKα radiation, scanning 2θ from 10 to 80°. Thermal analysis of the Al_2O_3 and Al_2O_3–ZrO_2 mixed oxides was carried out using an SDT Q600 simultaneous TGA-DSC instrument. Measurements were performed at a heating rate of 10°C min^{-1} up to 1000°C in air at 100 ml min^{-1}. Microstructural characterization of the supports was made in a scanning electron microscope (SEM, JEOL JSM-6400) with an acceleration voltage of 20 kV. The microstructure of catalysts was studied by transmission electron microscope (TEM) images obtained on a Philips Tecnai F20 (field emission scanning electron microscope (FESEM)) instrument operated at an accelerating voltage of 200 kV.

The coke deposited on the used catalysts was detected by DTA analysis, which was carried out with a Netzsch, STA-409EP thermal analyzer. It was performed from room temperature to 1000°C at a heating rate of 10°C min^{-1} in static air.

2.3 *Catalytic evaluation of Ni/Al–Zr catalysts*

The steam reforming reaction of ethanol (SRE) reaction was conducted in a fixed-bed quartz reactor with an inner diameter of 10 mm using 50 mg of catalyst. The catalysts were activated *in situ* by a reduction step at atmospheric pressure under H_2 flow (40 ml min^{-1}) at 650°C for 2 h. Steam reforming measurements were conducted at 500°C and at atmospheric pressure. The product mixture was analysed by an on-line gas chromatograph (GC), equipped with a flame ionization detector (FID) and a thermal conductivity detector (TCD).

3. Results and discussion

3.1 *Textural properties*

The nitrogen adsorption–desorption isotherms for Al_2O_3, Al_2O_3–ZrO_2 mixed oxides and Ni catalysts heat-treated at 700°C are shown in figure 1. In this figure, all isotherms of the supports and Ni catalysts are type IV, profiles characteristic of mesoporous materials. The hysteresis loops in these curves are E-type according to IUPAC, these indicate the existence of tubular pores with narrow openings, or inkwell type pores.

The pore-size distribution of the supports and Ni catalysts are shown in figure 2. The results indicate that only a unimodal pore-size distribution is obtained in the supports and catalysts [16]. Actually, the incorporation of small amounts of zirconia to alumina does not affect the average pore-size distribution; with the increasing zirconia content in the mixed oxides, the average pore-size distribution becomes smaller [17], as seen in figure 2a. The average diameter pore-size distribution of the supports varies from 54 Å toofpure alumina to 45 Å for the mixed oxide, which is richer in zirconium content (0.25Al–Zr).

The average pore-size distribution for the Ni-catalysts shows the same effect as the supports as seen in figure 2b, in which the average pore diameter ranges from 50 Å for the Ni–Al–Zr catalyst to 42 Å for the Ni–0.25Al–Zr catalyst. When comparing the distribution of the pore-size for the supports and catalysts, it may be seen that those are very similar, which in turn suggests that the dispersion of nickel metal load on the supports was homogeneous.

The specific surface areas of the supports and catalysts heat-treated at 700°C, as well as average pore diameter and pore volume are summarized in table 1. The surface area of the

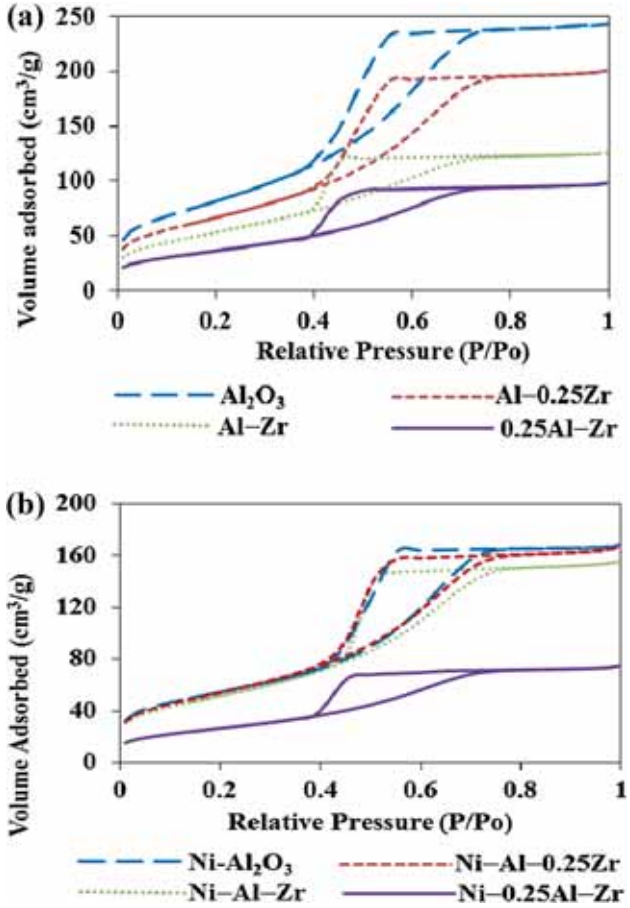

Figure 1. N_2 adsorption–desorption isotherms: (**a**) supports and (**b**) Ni-catalysts, heat-treated at 700°C.

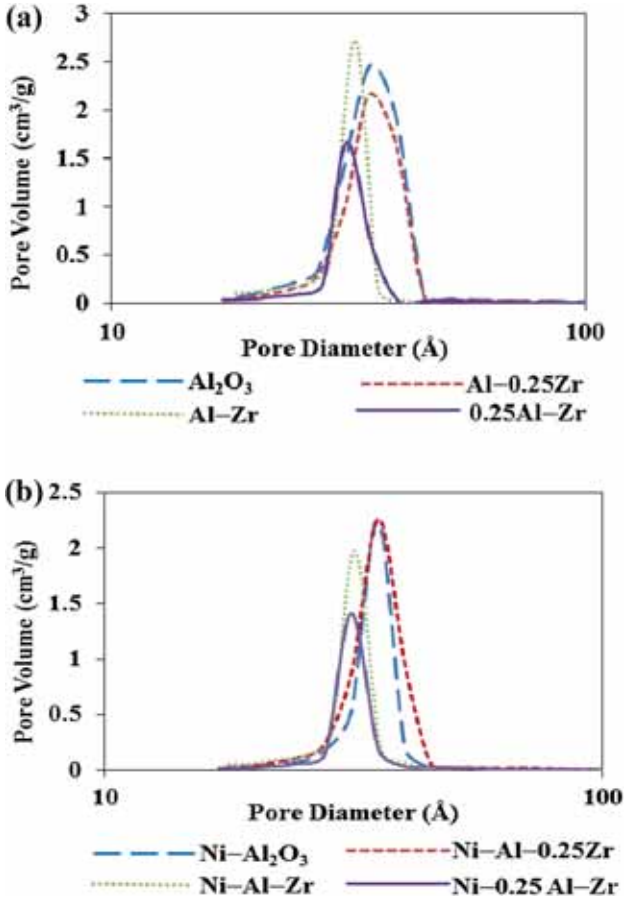

Figure 2. Pore-size distribution: (**a**) supports and (**b**) Ni-catalysts, heat-treated at 700°C.

supports (from 295 to 132 $m^2\ g^{-1}$) and catalysts (from 210 to 95 $m^2\ g^{-1}$) are decreased with the increment in the content of zirconium [18,19]; this is due to a diminution in the γ-Al_2O_3 content with high surface area, caused by the addition of ZrO_2 to the Al_2O_3. The same trend is present in the pore volume and average pore diameters in the supports and Ni-catalysts.

3.2 *XRD analysis*

The X-ray diffraction pattern (XRD) of the Al_2O_3 and Al–Zr mixed oxides heat-treated at 700°C are presented in figure 3. In the Al_2O_3 support, two small lumps at 2θ-46° and 2θ-66° corresponded to diffractions of γ-Al_2O_3 as shown in figure 3a. However, no intense peaks are observed because the synthesized alumina has an incipient ordered structure.

The three Al–Zr mixed oxides are synthesized as shown in figure 3b–d, there was no clear characteristic peak corresponding to the spectrum of the Al_2O_3 support, indicating that ZrO_2 was highly dispersed into alumina, thereby forming a solid solution. A moderate plateau of tetragonal ZrO_2 is shown at 2θ-30° in the mixed oxides, which increased with increasing zirconia content. However, the plateau was also considered as the appearance of amorphous zirconia [19, 20]. Therefore, the mixed oxides are amorphous with the 0.25Al–Zr oxide presenting an incipient crystallinity as observed in figure 3d.

Table 1. Textural properties of Al_2O_3–ZrO_2 supports and Ni catalysts heat-treated at 700°C.

Sample	S_{BET} ($m^2\ g^{-1}$)	D_p (Å)	V_p ($cm^3\ g^{-1}$)
Al_2O_3	295	53	0.5
Al–0.25Zr	240	51.5	0.46
Al–Zr	190	50	0.41
0.25Al–Zr	130	44.6	0.35
Ni–Al_2O_3	210	50	0.41
Ni–Al–0.25Zr	195	51	0.41
NiAl–Zr	140	46	0.33
Ni–0.25Al–Zr	95	42.3	0.18

Figure 4 shows the XRD spectra of catalysts with 10 wt% heat-treated at 700°C. Four peaks at 2θ: 37.2, 44, 63 and 75.5° are attributed to the (111), (200), (220) and (311) planes of

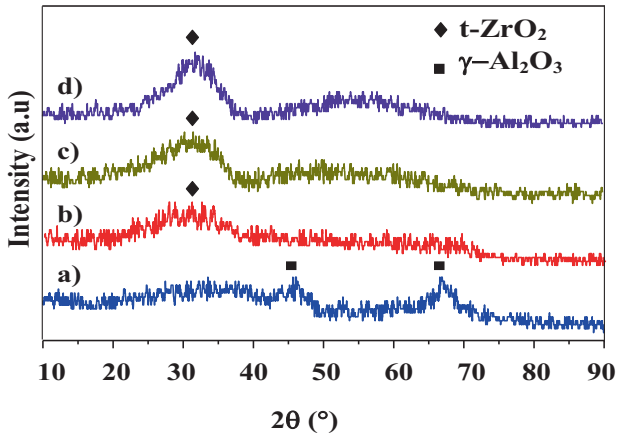

Figure 3. XRD patterns of supports heat-treated at 700°C: (**a**) γ-Al_2O_3, (**b**) Al–0.25Zr, (**c**) Al–Zr and (**d**) 0.25Al–Zr.

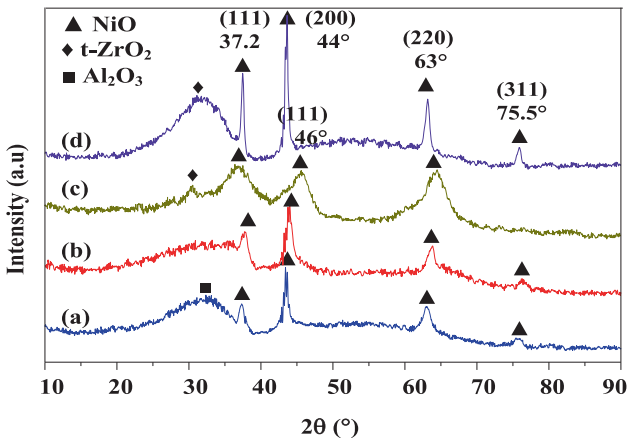

Figure 4. XRD patterns of Ni-catalysts: (**a**) Ni–Al_2O_3, (**b**) Ni–Al–0.25Zr, (**c**) Ni–Al–Zr and (**d**) Ni–0.25Al–Zr.

NiO in the crystalline phase, respectively, and are observed on the Ni catalysts [21]. The Ni − Al_2O_3 catalyst also shows a small shoulder at $2\theta \approx 32°$ that may result from the gamma phase alumina, due to the second heat treatment. This shoulder may also be due to the interaction of Ni with alumina to form the crystalline phase $NiAl_2O_4$, which has a stable and desirable structure, and is difficult to reduce [22].

The Ni–0.25Zr–Al_2O_3 catalyst does not present a clear diffraction peak for ZrO_2, indicating that the ZrO_2 was highly dispersed into alumina. However, the peak at 2θ of 30.5° of tetragonal ZrO_2 present in the Al–Zr and 0.25Al–Zr supports appears at 2θ of 31.5 and 32° in the XRD spectra of the Ni–Al–Zr and Ni–0.25Al–Zr catalysts, respectively. This is because of the lattice of ZrO_2 is contracted by the incorporation of Al^{+3} ions into ZrO_2 [23]. The diffraction intensities of the NiO crystals have become stronger by increasing the content of zirconium in mixed oxides of Al_2O_3–ZrO_2, indicating that Ni^{+2} ions interact more strongly with the alumina as zirconia content is increased.

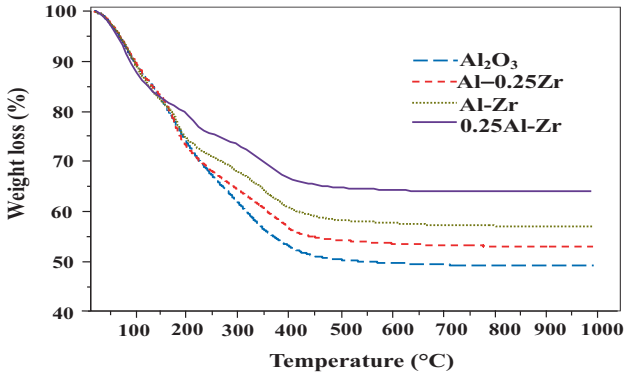

Figure 5. TGA curves of the Al_2O_3–ZrO_2 supports.

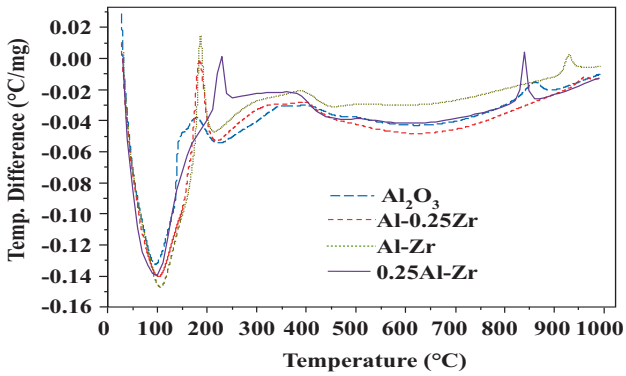

Figure 6. DTA of Al_2O_3–ZrO_2 supports.

3.3 *Thermal analysis*

Thermal analyses of the fresh supports are illustrated in figure 5. In the thermogravimetric analysis (TGA) curve for the pure alumina, the weight loss percentage from room temperature to 150°C was measured about 15.1%, which is consistent with a broad endothermic peak in the DTA curve, as seen in figure 6. This result is attributed to the elimination of residual water and physically adsorbed ethanol. A second weight loss, about 19.7%, was measured at 150 − 262°C in the TGA curve, which is represented by an exothermic peak in the DTA curve and can be attributed to the incipient combustion of residual organic compounds (alkoxides) synthesis. The third weight loss (9.7%) from 262 to 379°C is associated with an exothermic peak in the DTA curve, and is related to dehydroxylation of the boehmite to the γ-Al_2O_3 phase [17,24].

Between 379 and 440°C, a fourth weight loss (3.1%) occurs in the TGA curve, which is associated with the combustion of occluded organic molecules [25,26], and is represented by a small exothermic peak in the DTA curve. In the temperature range of 440–510°C, a fifth weight loss of about 1.2% occurs, which is represented by a change in the exothermic DTA curve, and is associated with the final formation of γ-Al_2O_3 [27], as seen in the XRD analyses. The TGA curve

shows a small weight loss (∼0.3%) between 800 and 900°C related with a small exothermic peak, and should be attributed to the crystallization of alumina.

The fresh Al_2O_3-ZrO_2 mixed oxides show five weight losses in the TGA curve. In the range of 27−120°C, the weight loss of 16, 18.2 and 19.1% in the Al–0.25Zr, Al–Zr and 0.25Al–Zr supports, respectively, correspond to the first broad endothermic peak in the DTA curve, and is ascribed to the evaporation of ethanol and adsorbed water from the Al_2O_3–ZrO_2 mixed oxides. Between 170 and 240°C, a second weight loss occurs (3.1%) in the TGA curve for Al_2O_3–ZrO_2 mixed oxides with weight loss about 17.8, 11.8 and 5.8%. In the aforementioned order of the mixed oxides, which is mainly associated with the initial combustion of alkoxides (aluminum tri-sec-butoxide and zirconium (IV) propoxide), and is represented by a change in the exothermic DTA curve. In the 0.25Al–Zr support, this exothermic peak (centred at around 210°C) is observed and is shifted to the right in the DTA curves, indicating that initial combustion is mainly due to the burning of aluminum tri-sec-butoxide. The third weight loss (∼6.2 and ∼6.8%) was measured from 240 to 360°C in the Al–0.25Zr and Al–Zr supports, respectively, is related to a small exothermic peak in the DTA curve, and is associated with the elimination of chemically bonded water [17]. Another small exothermic peak is observed in the DTA curve at about 400°C for Al–0.25Zr and Al–Zr supports, which can be attributed to the tetragonal phase of ZrO_2. This result represents the fourth weight loss of about 5.7 and 5.3% in the TGA curve for the Al–0.25Zr and Al–Zr supports, which was observed in XRD results.

On the other hand, the TGA curve of 0.25Al–Zr support the third and fourth weight losses (∼8.5%) that are observed only at a temperature range of 210 − 410°C. Finally, a weight loss for all mixed oxides occurs between 800 and 1000°C, represented by a small exothermic peak in the DTA curve, corresponding to the transformation of the tetragonal into the monoclinic zirconia phase [19,28].

3.4 *SEM analysis*

The microstructures of the supports of Al_2O_3–ZrO_2 were analysed by SEM as shown in figure 7. The images show that the supports are formed from mesoporous agglomerates of homogeneous-sized particles with a spherical shape, and with a rough size of 0.3 μm on the scale of resolution, indicating that the supports are amorphous, as evidenced by the XRD studies. It is evident that the particle size increases with

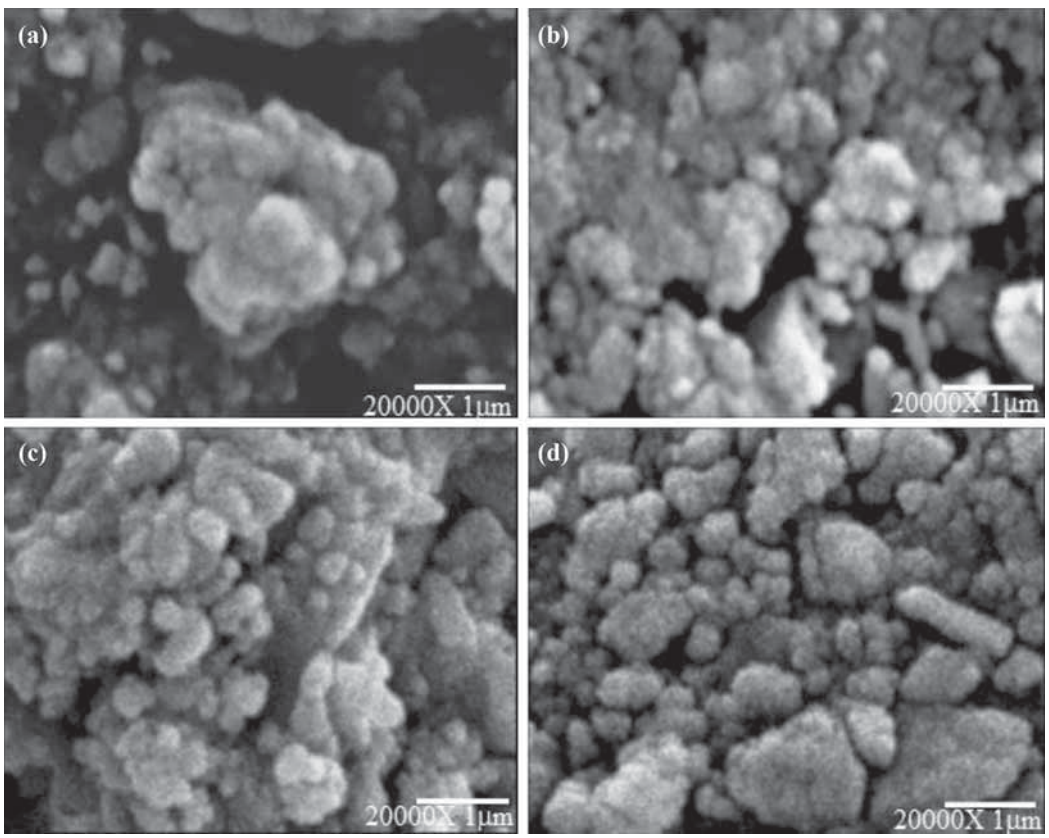

Figure 7. Micrograph by SEM of: (**a**) Al_2O_3, (**b**) Al–0.25Zr, (**c**) Al–Zr and (**d**) 0.25Al–Zr supports heat-treated at 700°C.

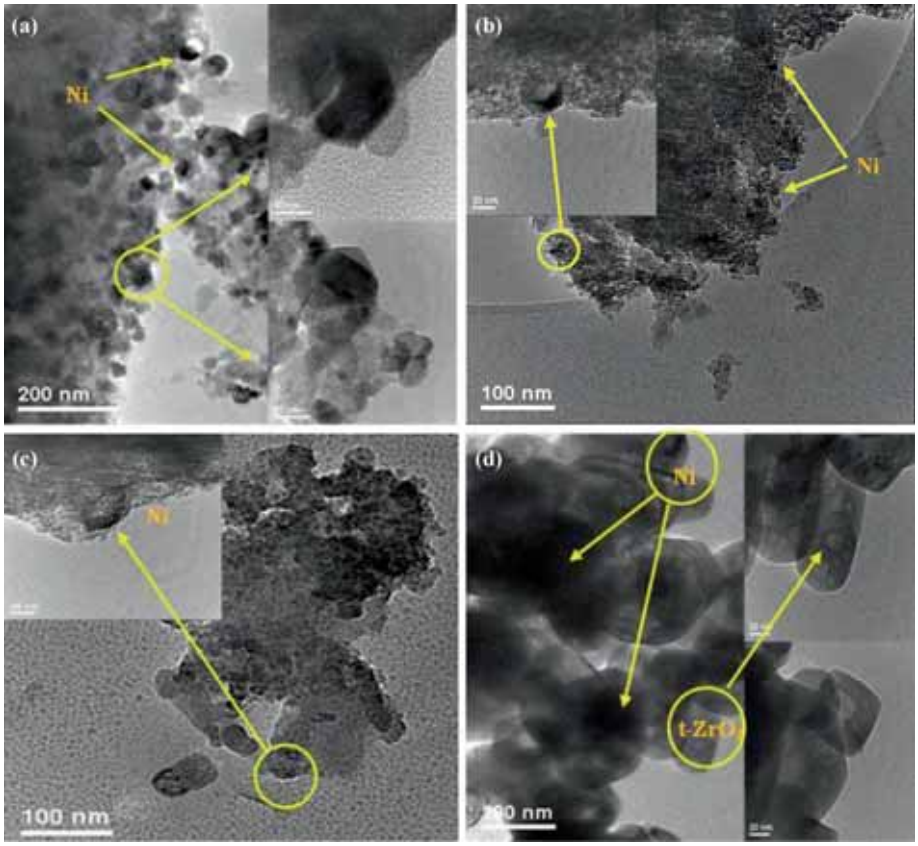

Figure 8. TEM micrographs of: (**a**) Ni–Al_2O_3, (**b**) Ni–Al–0.25Zr, (**c**) Ni–Al–Zr, (**d**) Ni–0.25Al–Zr heat-treated at 700°C.

increasing zirconia content, whereby the size of the agglomerates decreases; this is confirmed by the results obtained from BET analysis [29].

3.5 *TEM analysis*

Figure 8 shows the TEM micrographs of Ni-catalysts heat-treated at 700°C. The Ni–Al_2O_3 catalyst shows uniform distribution of metal particles (NiO) with an average size between 15 and 20 nm. The presence of NiO crystals is confirmed by XRD analysis for this catalyst in figure 4a. This uniform dispersion is also confirmed by BET analysis because the Ni–Al_2O_3 catalyst presents a high surface area.

In the TEM micrograph of the Ni–Al–0.25Zr catalyst which is represented in figure 8b, we can see that the addition of ZrO_2 to the alumina makes it more difficult to observe the distribution of NiO. It is more difficult because the zirconia can mask the NiO crystals, since Zr has a higher electron density than nickel. This result is also observed in the catalyst of Ni as shown in figure 8c, with NiO crystals in the range of 20– 30 nm. Finally, in the TEM micrograph of Ni–0.25Al–Zr catalyst, crystalline zirconia can be distinguished (figure 8d), which correspond t–ZrO_2 according to the results of XRD (figure 4d).

3.6 *Catalytic evaluation*

The SRE was performed at 500°C with an S/E ratio of 3:1. The basic reaction scheme is as follows:

$$C_2H_5OH + 3H_2O \rightarrow 2CO_2 + 6H_2. \quad (1)$$

Figure 9 shows ethanol conversion as a function of time over different Ni–Al–Zr catalysts.

The ethanol conversion reached by the Ni–Al–0.25Zr catalyst is 91%, showing selectivity to hydrogen, carbon dioxide, carbon monoxide and methane of 55.7, 25, 14.1 and 2.8%, respectively, traces of ethylene and acetaldehyde also were detected (2.3%) as shown in figure 10b. Similar results are obtained with the Ni–Al–Zr catalyst as seen in the figure 10c. On the other hand, the ethanol conversion reached by the Ni–Al_2O_3 catalyst is 88% after 3 h of reaction with a selectivity of ∼52.8, 24.2, 17.1, 3 and 2.9% for H_2, CO_2, CO, CH_4, traces of CH_3CHO and C_2H_4, respectively (figure 10a).

The presence of a higher concentration of CO_2 in the reaction products indicates a methane decomposition reaction of ethanol (equation (2)) and subsequent reforming of methane with steam to form CO_2 (equation (3)) [30–32]:

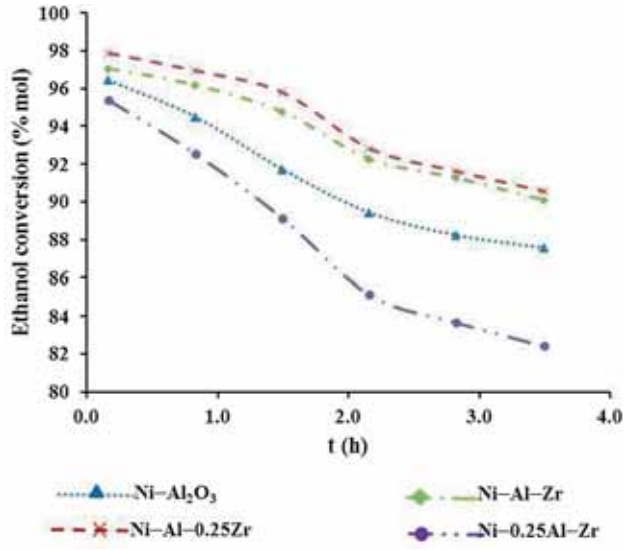

Figure 9. Conversion of ethanol as a function of time on steam reforming reaction for Ni–Al–Zr catalysts.

$$C_2H_5OH \rightarrow CH_4 + CO + H_2, \quad (2)$$

$$CH_4 + 2H_2O \rightarrow 4H_2 + CO_2. \quad (3)$$

The gas shift water reaction (WGS) can also occur to form hydrogen and carbondioxide (equation (4)):

$$CO + H_2O \leftrightarrow CO_2 + H_2. \quad (4)$$

The presence of traces of ethylene and acetaldehyde in the reaction products indicate that an ethanol dehydration to ethylene (equation (5)) and ethanol dehydrogenation to acetaldehyde (equation (6)) can also occur:

$$C_2H_5OH \rightarrow CH_3CHO + H_2, \quad (5)$$

$$C_2H_5OH \rightarrow C_2H_4 + H_2O. \quad (6)$$

Furthermore, acetaldehyde and ethylene in the reforming reaction produce more hydrogen and carbon monoxide equations (7 and 8):

$$CH_3CHO + H_2O \rightarrow 3H_2 + 2CO, \quad (7)$$

$$C_2H_4 + 2H_2O \rightarrow 2CO + 4H_2. \quad (8)$$

The minimum ethanol conversion and selectivity to the products of reaction occurs in Ni–0.25Al–Zr catalyst (which is richer in zirconia content), reaching a value of ∼82.3% after 3.5 h of reaction, attributed to increased formation of coke in this catalyst (figure 10d). This is due to traces of ethylene (1.8%) and acetaldehyde (2.3%) found in the reaction products, which in turn is the precursor of coke formation (equation (9)) and particle size [32]. According to the results of TEM, this catalyst is richer in zirconia content and has a larger particle size, which is less likely to account for the active sites.

$$C_2H_4 \rightarrow \text{polymerization} \rightarrow \text{coke}. \quad (9)$$

Carbon deposits can also be formed by the Boudouard reaction (equation (10)) and consecutive dehydrogenation of methane (equation (11)):

$$2CO \leftrightarrow CO_2 + C, \quad (10)$$

$$CH_4 \rightarrow CH_3 \rightarrow CH_2 \rightarrow CH \rightarrow C. \quad (11)$$

The results of the SRE indicate that the incorporation of optimal amounts of zirconia into the Ni/Al_2O_3 catalyst provides a strong metal–support interaction, increasing its stability due to higher nickel dispersion on the alumina surface and neutralizing the acidity of the catalyst [33]. Thus, the Ni–Al–0.25Zr catalyst shows a higher selectivity towards hydrogen due to faster the ethylene and acetaldehyde reforming reactions. In this way, the deactivation of Ni–Al–0.25Zr catalyst is less than the $Ni-Al_2O_3$ catalyst.

On the other hand, the incorporation of higher amounts of ZrO_2 in the Ni/Al_2O_3 catalyst decrease the surface area of catalyst, which results in weaker metal–support interactions in the Ni–0.25Al–Zr catalyst, leading to low dispersion of Ni particles [34]. This increase in the Ni particle size results in a lower selectivity towards hydrogen due to major production of ethylene and acetaldehyde in the reaction products, which causes a fast deactivation of the Ni–0.25Al–Zr catalyst by coke formation.

The performance of various Ni/Al_2O_3, Ni/ZrO_2 and Ni/Al–Zr catalysts in SRE is summarized in table 2. For the same operating conditions, the Ni–Al–0.25Zr catalyst proposed in this study is more selective to hydrogen than the Ni–Al_2O_3 and Ni/ZrO_2 catalysts of the references. However, the reforming temperature, nickel loading and the molar ratio of water–ethanol play an important role in the conversion of ethanol and selectivity to hydrogen in the SRE as seen in table 2.

3.7 *Characterization of used catalysts*

The results of coke nature characterization by DTA analysis are shown in figure 11. The DTA profile of the coke deposited on the used Ni–0.25Al–Zr catalyst shows three combustion peaks at 380, 680 and 850°C, respectively. The peak at 380°C evidences the presence of amorphous coke (monoatomic and polymeric carbon) that is adsorbed on the metal sites and cover them (encapsulating carbon) [41,42], which results in a rapid deactivation and low selectivity to H_2 as shown in figures 9 and 10d, respectively. This type of carbon may be attributed to polymeric carbon originating from ethylene polymerization

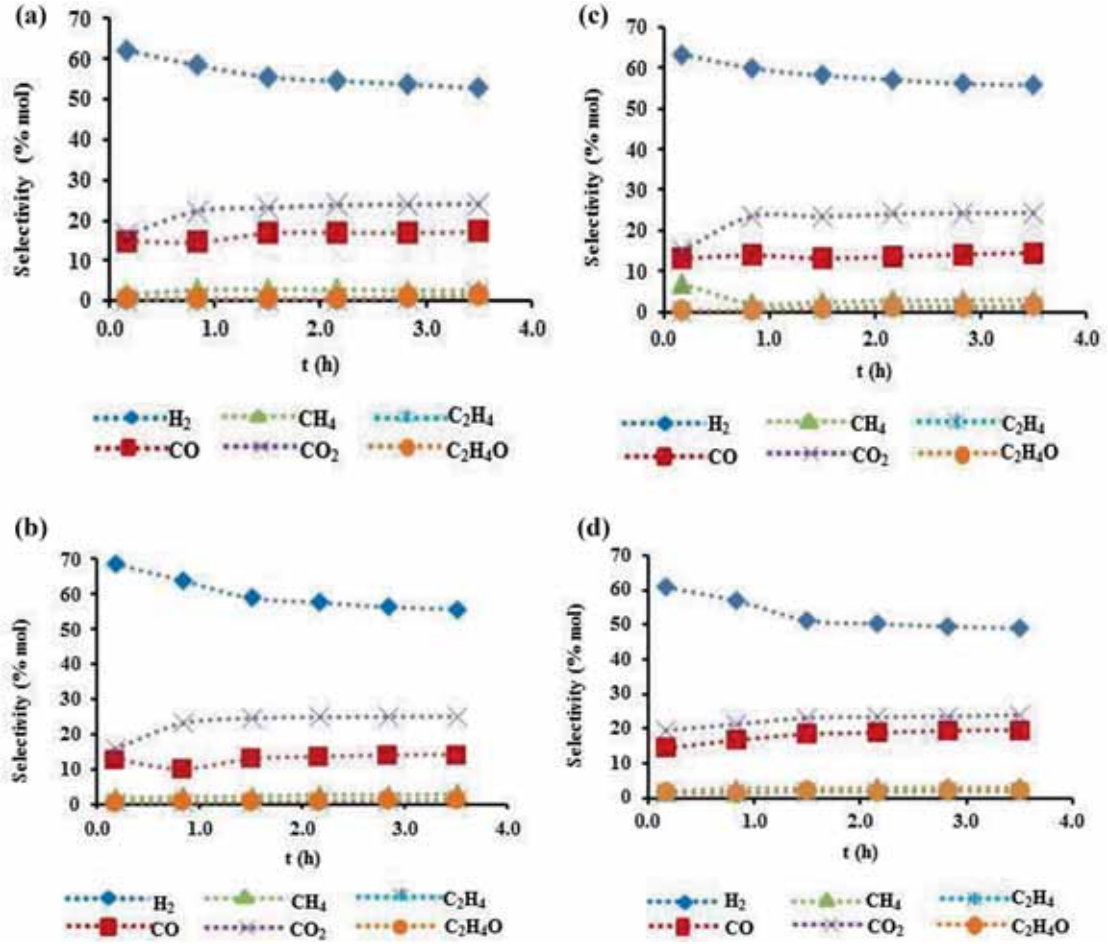

Figure 10. Product distribution for SRE over: (**a**) Ni–Al_2O_3, (**b**) Ni–Al–0.25Zr, (**c**) Ni–Al–Zr and (**d**) Ni–0.25Al–Zr catalysts at 500°C.

Table 2. The performance of Ni/Al_2O_3 and Ni/ZrO_2 catalysts in SRE.

Catalyst	Ni ($\%_w$)	Temperature (°C)	H_2O/EtOH (mol mol^{-1})	t (h)	EtOH conversion (%)	S_{H_2} (%)	Reference
Ni–Al	35	500	3.3	6	100	~60	[35]
Ni–Al	17.4	550	3:1	4.1	100	15	[36]
Ni–Al	16	500	3:1	4	100	~57	[34]
Ni–Al	15	450	6:1	NR	100	50	[37]
Ni–Al	10	500	3:1	9	NR	30	[38]
Ni–Al	10	500	4:1	2	100	55	[39]
Ni–Al	10	400	6:1	3	100	63.64	[40]
Ni–Zr	10	500	3:1	9	NR	51	[38]
Ni–Al–0.25Zr	10	500	3:1	3	91	55.7	Present study

NR = not reported.

and acetaldehyde decomposition reactions. The combustion peaks at 680 and 850°C correspond to the oxidation of a highly graphitic coke [43].

The DTA profile of the coke deposited on the used Ni–Al_2O_3 catalyst shows two combustion peaks at 430 and 650°C, which correspond to a polymeric and graphitic coke, respectively. Polymeric carbon is first observed at a temperature of 380°C in the Ni–0.25Al–Zr catalyst, while in the Ni–Al_2O_3 catalyst, it is observed up to 430°C, this is the reason which catalyst activity in the Ni–0.25Al–Zr catalyst is

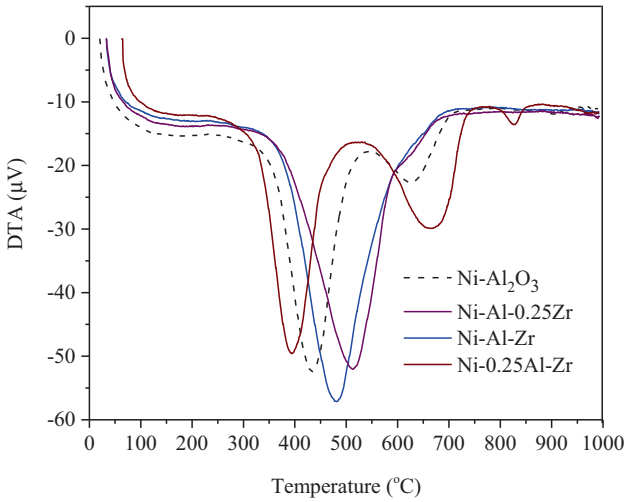

Figure 11. DTA profiles of the used catalysts in SRE at 500°C.

minor, because the coke encapsulates the Ni particles more rapidly in this catalyst.

The DTA profile of the used Ni–Al–0.25Zr and Ni–Al–Zr catalysts show a single combustion peak at 490 and 520°C, respectively, which correspond to filamentous coke (whisker-type carbon) with different graphitization degrees, formed mainly from the Boudouard (equation (10)) and consecutive dehydrogenation of methane reactions (equation (11)) [31,33,44], which do not block metal sites and not necessarily cause a loss of intrinsic catalyst activity. Therefore, this type of carbon allows regeneration of catalysts and its formation occurs at temperatures above 450°C [41].

4. Conclusions

The characterization results of the Al_2O_3–ZrO_2 mixed oxides prepared by sol–gel method showed that the addition of ZrO_2 into Al_2O_3, reduced the specific surface area, increasing the content of zirconium according to BET analysis. XRD patterns do not clearly identify well-defined crystalline structures corresponding to ZrO_2 or Al_2O_3 for molar ratios (Al_2O_3/ZrO_2) of 1:1, 0.25:1, and this result in turn suggests that the samples are mostly amorphous solids. However, higher molar ratios of ZrO_2/Al_2O_3 show that this fact may be identified as incipient crystallization in the mixed oxide, which is due to the tetragonal phase of zirconia. This phase was clearly characterized in the TGA of the 0.25Al–Zr support. The SEM analysis of mixed oxides reveals that the size of the particles increases by increasing the content of zirconium, directly affecting the crystallinity of the nickel catalysts according to the results obtained by XRD and TEM.

Ni has high activity for C–C, O–H and C–H bonds breaking, facilitating H atoms to form molecular H_2 and converting CO to CO_2. However, the Ni catalyst suffers from coke formation as well as metal sintering, leading to rapid deactivation in SRE. The Al_2O_3 is a support with strong acidic nature, which promotes dehydration reaction of ethanol to ethylene causing the formation of amorphous coke and deactivating the Ni particles rapidly. The ZrO_2 was introduced to alumina to improve the Ni–Al_2O_3 catalyst stability by suppressing the acidity of carrier and minimized the dehydration of ethanol on the alumina support.

The activity of the studied catalysts of Ni indicates that conversion of ethanol and selectivity towards H_2 in the SRE, progressively decreases with the increment in zirconia content. This is due to the increase of the mean particle size and crystallinity, resulting in further formation of coke by the ethylene route in the ethanol reforming reaction. The DTA results of the used catalysts indicate that optimal incorporation of ZrO_2 into the Ni–Al_2O_3 catalyst improves its stability and resistance to the formation of polymeric coke (below 450°C). The deposited coke is filamentous (formed above 450°C through Bourduard reaction and consecutive dehydrogenation of methane), which does not encapsulate the nickel particles and has a minor effect on the deactivation of the catalyst by coke, allowing its regeneration. Therefore, the proposed catalyst can also be used in reforming the natural gas or other hydrocarbons.

Acknowledgements

J Angel-Soto expresses thanks to the University of Guanajuato and to CONACYT, for the financial support granted to this project.

References

[1] Chen X, Liu Y, Niu G, Yang Z, Blan M and He A 2001 *Appl. Catal. A: General* **205** 159
[2] Khalaf H A 2013 *SpringerPlus* **2** 1
[3] Dabbagh H A and Zamani M 2011 *Appl. Catal. A: General* **404** 141
[4] Davies L E, Bonini N A, Locatelli S and Gonzo E E 2005 *Lat. Am. Appl. Res.* **35** 23
[5] Liu X, Lu G and Yan Z 2003 *J. Nat. Gas Chem.* **12** 161
[6] Teterycz H, limkiewicz R K and Laniecki M 2003 *Appl. Catal. A: General* **249** 313
[7] Ortiz-Landeros J, Contreras García M E and Pfeiffe H 2007 *Adv. In Tech. Mat. Mat. Proc.* **9** 119
[8] Hong D Y, Vislovskiy V P, Park Y H and Chang J S 2006 *Bull. Korean Chem. Soc.* **27** 789
[9] Chary K V R, Kumar Ch P, Rao P V R and Rao V V 2004 *Catal. Commun.* **5** 479
[10] Seo J G, Youn M H, Park S, Chung J S and Song I K 2009 *Int. J. Hydrogen Energ.* **34** 3755
[11] Li H and Wang J 2004 *Chem. Eng. Sci.* **59** 4861
[12] Ping H Z, Chun H, Zheng J and Lu G Q 2004 *J. Environ. Sci. (China)* **16** 316
[13] Carmo Rangel M, Paternina Berrocal G, Maciel C G and Mansu Assaf J 2011 *Adv. Chem. Res.* **10** 341
[14] Wang S and Lu G 1998 *Appl. Catalysis—B: Environ.* **16** 269

[15] Iriondo A, Barrio V L, Cambra J F, Arias P L, Güemez M B, Navarro R M *et al* 2008 *Top. Catal.* **49** 46
[16] Angel J, Aguilera A F, Galindo I R, Martinez M and Viveros T 2012 *Mater. Sci. Appl.* **3** 650
[17] Klimova T, Rojas M L, Castillo P, Cuevas R and Ramirez J 1998 *Micropor. Mesopor. Mater.* **20** 293
[18] Chen Y W, Yen T M and Li C 1995 *J. Non-Cryst. Solids* **185** 49
[19] Li G, Li W, Zhang M and Tao K 2004 *Catal. Today* **93–95** 595
[20] Sarkar D, Mohapatra D, Ray S, Bhattacharyya S, Adak S and Mitra N 2007 *Ceram. Int.* **33** 1275
[21] Cai M, Wen J, Chu W, Cheng X and Li Z 2011 *J. Nat. Gas Chem.* **20** 318
[22] Ding R G and Yan Z F 2002 *Fuel Chem. Division Preprints* **47** 108
[23] Youn M H, Seo J G, Jung J C, Park S and Song I K 2009 *Int. J. Hydrogen Energ.* **34** 5390
[24] Liu Q, Wang A, Wang X, Gao P, Wang X and Zhang T 2008 *Micropor. Mesopor. Mater.* **111** 323
[25] Tursiloadi S, Imai H and Hirashima H 2004 *Indonesian J. Chem.* **4** 149
[26] Kirszensztejn P and Szymkowiak A 2005 *J. Therm. Anal. Calorim.* **81** 35
[27] Perez-Pastenes H, Ochoa-Tapia A and Viveros T 2006 *J. Sol-Gel Sci. Technol.* **37** 49
[28] Zawadzki M, Hreniak D, Wrzyszcz J, Mista W, Grabowska H, Malta O L *et al* 2003 *Chem. Phys.* **291** 275
[29] Nouri E, Shahmiri M, Rezaie H R and Talayian F 2012 *Int. J. Ind. Chem.* **3** 1
[30] Benito M, Sanz J L, Isabel R, Padilla R, Arjona R and Daza L 2005 *J. Power Sources* **151** 11
[31] Fatsikostas A N and Verykios X E 2004 *J. Catal.* **225** 439
[32] Cavallaro S 2000 *Energy Fuels* **14** 1195
[33] Sanchez-Sanchez M C, Navarro R M and Fierro J L 2007 *Int. J. Hydrogen Energ.* **32** 1462
[34] Pompeo F, Nichio N N, Souza M M V M, Cesar D V, Ferretti O A and Schmal M 2007 *Appl. Catal. A: General* **316** 175
[35] Comas J, Marino F, Laborde M and Amadeo N 2004 *Chem. Eng. J.* **98** 61
[36] Fajardo H V, Longo E, Mezalira D Z, Nuernberg G B, Almerindo G I *et al* 2010 *Environ. Chem. Lett*. **8** 79
[37] Liberatori J W C, Ribeiro R U, Zanchet D, Noronha F B and Bueno J M C 2007 *Appl. Catal. A: General* **327** 197
[38] Saeki T, Ohkita H, Kakuta N and Mizushima T 2015 *J. Jpn. Petrol. Inst.* **58** 341
[39] Denis A, Grzegorczyk W, Gac W and Machocki 2008 *Catal. Today* **137** 453
[40] Bshish A,Yaakob Z, Ebshish A and Alhasan F H 2013 *ASME J. Energy Resour. Technol.* **136** 012601
[41] Bartholomew C H 2001 *Appl. Catal. A: General* **212** 17
[42] Montero C, Valle B, Bilbao J and Gayubo A 2014 *Chem. Eng. Trans.* **37** 481
[43] Vicente J, Montero C, Ereña J, Azkoiti M J, Bilbao J and Gayubo A G 2014 *Int. J. Hydrogen Energ.* **39** 12586
[44] Cheng H, Feng S, Tao W, Lu X, Yao W, Li G *et al* 2014 *Int. J. Hydrogen Energ.* **39** 12604